IEEE Access
Multidisciplinary | Rapid Review | Open Access Journal

Received October 29, 2019, accepted November 14, 2019, date of publication November 20, 2019,
date of current version December 11, 2019.

Digital Object Identifier 10.1109/ACCESS.2019.2954626

Recognition of Angiographic Atherosclerotic Plaque Development Based on Deep Learning

JINYONG ZHAN, JUE WANG, ZHIFEI BEN, HAIDONG RUAN, AND SAIJUN CHEN
HwaMei Hospital, University of Chinese Academy of Sciences, Ningbo 315010, China

Corresponding author: Zhifei Ben (nbzxycs@126.com)

This work was supported by the Dual Ligand Targeting Microbubbles with Sialyl Lewisx and Anti-E-Selectin Monoclonal Antibody Zhejiang Medicine and Health Sciences Research Fund, under Grant 2019RC077.

ABSTRACT In order to obtain accurate information on the degree of plaque development in patients' blood vessels, and to assist clinicians in judging and recognizing atherosclerotic areas, a deep learning-based study of intravascular ultrasound atherosclerotic plaque development was performed (CPCA). First, different types of ROIs are extracted for plaque images. Secondly, according to different ROI regions, the size of the sliding neighborhood block is determined, and the central pixel traverses the plaque region to obtain a small image slice of the plaque developing region. Then, based on PCAnet based on principal component analysis vector as convolution kernel, a clustering PCA network is designed to cluster small image slices and calculate principal component vectors by category to generate multiple sets of convolution kernels. The multi-plaque visualization feature enables the input image to adaptively select the feature extractor to achieve classification recognition of the degree of plaque development. The result of manual labeling by doctors is taken as the standard true value. The experimental results show that the proposed algorithm can effectively extract the features of plaque developed images and achieve high-efficiency recognition of plaque development.

INDEX TERMS Deep learning, plaque, degree of development, recognition.

I. INTRODUCTION

Coronary artery disease (CAD) is commonly known as Coronary atherosclerotic heart disease [1]. Due to severe atherosclerosis or spasm in the coronary artery, the coronary artery is narrowed or blocked, forming thrombus, causing the lumen to block, and finally unable to provide cardiac nutrition, resulting in myocardial infarction due to insufficient blood supply and oxygen supply. Clinically, the prominent manifestations are acute myocardial infarction, unstable angina pectoris, gangrene, thrombosis, peripheral function loss, and so on [2], which is a kind of sudden cardiovascular disease with high risk and high mortality.

With the rapid development of modern electronic technology and clinicians, the diagnosis of coronary heart disease (CHD) was thoroughly discussed by relevant researchers. People, they are from the early diagnosis of coronary artery disease, caused by myocardial infarction and insufficient coronary artery blood supply from typical clinical symptoms and signs, to electrocardiogram characteristics and myocardial enzyme examination. Later, new technologies and equipment such as radionuclide examination, coronary angiography, echocardiography, intravascular ultrasound, and optical coherence tomography were gradually developed. Among them, the most widely used clinically and most mature imaging methods are Coronary Angiography (CAG) [3] and Intravascular Ultrasound (IVUS) [4]. The IVUS acquires images of the lumen of the blood vessel and the wall of the vessel during catheter withdrawal by placing a tiny ultrasound probe at the tip of the catheter into the vessel. At present, IVUS can provide visual observation and detection of blood vessels for clinical use, help to obtain information such as the degree of development of atherosclerotic plaque. And then, it can judge and identify the degree of development of plaque, thus the stability and risk of plaque. Sexually conduct an effective assessment.

Since the ultrasonic echoes of different tissue structures in the lumen are different, the IVUS image can show the structure of the vessel wall. Clinically, doctors mainly identify and judge the degree of development of plaque based on experience, so they are subjective. In recent years, new IVUS technologies have developed rapidly, such as Virtual Histology IVUS (VH-IVUS) and IVUS Elastography (IVUS-E). The VH-IVUS technique utilizes

The associate editor coordinating the review of this manuscript and approving it for publication was Yongtao Hao.

backscattered ultrasound RF signals to perform feature extraction to identify plaque development by power spectral processing, including Fourier transform, welch power spectrum, and autoregressive models. Although this method can classify the degree of plaque development and reconstruct tissue histological images similar to histopathological sections [5], [6], it still has limitations. For example, the recognition ability of borders in VH-IVUS images is poor, usually requires manual Calibrated and the image reconstruction time is longer. IVUS-E evaluates the development of plaque by detecting the characteristics of plaque in the arteries [7], but it is difficult to distinguish between fibrous tissue and lipid tissue, and the relationship between plaque rupture rate and rupture position is not clear. The IVUS image is rich in texture and rich in gray-scale information [8], [9]. It can extract multiple image features, and based on these feature values, the degree of development of intravascular plaque can be identified. At present, there are many feature extraction methods, such as gray level co-occurrence matrix method, Gabor filter, Local Binary Pattern (LBP), and so on. The features extracted by the gray level co-occurrence matrix method can be used for plaque regions in IVUS images. The analysis of local patterns and permutation rules, but only the gray-scale co-occurrence matrix method for classification and identification of IVUS image patches, it is difficult to distinguish fibrosis and lapidated plaques [10]. GAO [11] et al. classify the gray level co-occurrence matrix of the developed regions extracted by different plaque tissues by using Haralick texture statistics. Lian and Huang [12] combined gray-scale co-occurrence matrix and gray-gradient co-occurrence matrix extraction features, design SVM classifier. The contrast classifier identifies the degree of development of plaque in the image under two feature value extraction methods. Liu *et al.* [13] combined contour transform and active contour model to carry out patch development image segmentation. Then, texture features were extracted and three classifiers, fisher, SVM and generalized correlation learning vector quantization, were designed to classify and compare the development of plaques. Based on RF data and image texture extraction features, Rocha and Goldenstein [14] use ECOC error correction coding samples and classify them into a variety of basic classifiers to achieve classification description of plaque development degree. Sampedro *et al.* [15] classify plaque images into three categories based on a multi-class multi-scale stack sequential learning method. This method has poor recognition performance for plaque development. Most of these methods are based on image region blocks for classification, and the properties of different plaque tissues are classified by extracting features of local images. The shortcomings are also obvious. In the method, a large number of feature engineering is needed to obtain the effective features related to plaque. And the classifier is designed to classify the plaques to achieve the purpose of organization and characterization.

Most of the current atherosclerotic plaque algorithms are classified and identified by traditional algorithms. However, its disadvantages are also obvious. In this method, a large number of feature extraction algorithms are needed to obtain effective features related to plaque, and then plaques are classified by designing a classifier to achieve the purpose of organizing and selecting plaques. Such an algorithm will increase the time consumption and is not conducive to the application in clinical medicine.

In 2006, Hinton first proposed ''deep learning'' [16], [17]. The deep learning network has a hierarchical structure, and the feature extraction is realized by layer-by-layer extraction features [18]. In addition, deep learning can better learn image features without supervision, and has been used by more and more scholars in the field of image processing [19]–[21]. Many scholars have applied deep learning, especially convolutional neural networks, to medical image processing, providing new ideas and research methods for medical image diagnosis [22], [23]. Araki *et al.* [24] used the emerging deep learning framework to construct a convolutional neural network, and automatically extracted the optimal feature parameters of different plaque components in the carotid IVUS image. And then, they input it into a nine-layer convolutional neural network for classification and recognition. The results of the verification show that a better recognition effect can be obtained. This method does not require excessive pre-processing and pre-extraction features, providing a more optimized solution for quickly and accurately automatically recognizing the degree of development of plaque. Shi *et al.* [25] used neural network methods to detect the degree of plaque development. The method first acquires the ROI using a morphological-based watershed algorithm. The gray values of the 3×3, 7×7, and 11×11 neighborhoods to be detected are then input to the three multilayer perceptions, respectively. The output of the three-layer perceptron is then input to the fourth multi-layer perceptron. The final multi-layered output is finally used as the final classification of the pixel. The algorithm has better anti-noise performance, and can still obtain better segmentation effect for ultrasonic images that are interfered by noise. However, the training process of the network is more complicated, and the actual hidden layer of the multi-layer perceptron used has only one layer. Too few layers are not conducive to extracting the essential characteristics of the input data, which is not conducive to subsequent classification. Hoseini *et al.* [26] applied CNN to the segmentation of plaque developed images. The algorithm has better segmentation effect, but the calculation process is complicated and time consuming. Hamwood *et al.* [27] proposed the segmentation problem of patch developing images with full convolutional neural network. In the process of image classification, the convolution layer in CNN extracts features from the image block of fixed size, and then gets a feature vector of fixed length through the full connection layer. The feature vector is input into the classifier (SVM or Softmax) to get the classification result. Soffer *et al.* [28] combined the scale space and multi-resolution statistical classification method of carotid ultrasound images, and then combined the CNN network to

classify and identify the plaque development images. Bao and Chung [29] adopted multi-scale CNN structure to apply it to the segmentation of plaque development images. This algorithm has a good segmentation effect and provides a new research direction for the classification and recognition of plaque development images.

However, there are still three main problems in the application of deep learning algorithms in medical images. First, deep learning networks require a large amount of data for training. However, the acquisition of medical image data is usually difficult and time consuming. Samples with real values are more difficult to collect. Secondly, deep learning networks usually require images of the same size as input, but the region of interest (ROI) in medical images is usually irregular and of different sizes. Due to the complexity of the medical image itself, even experienced doctors may draw different conclusions during the diagnosis process, which makes the deep learning network more difficult to train [30].

In this paper, angiographic contrast-enhanced atherosclerotic plaques were used as the research object, and a depth learning-based plaque development degree recognition algorithm was proposed. First, different types of ROIs are extracted for plaque images. Secondly, according to different ROI regions, the size of the sliding neighborhood block is determined, and the central pixel traverses the plaque region to obtain a small image slice of the plaque developing region. Then, based on PCAnet based on principal component analysis vector as convolution kernel, a clustering PCA network is designed to cluster small image slices and calculate principal component vectors by category to generate multiple sets of convolution kernels. The multi-plaque development feature enables the input image to adaptively select the feature extractor for classification recognition.

Specifically, the technical contributions of our paper can be concluded as follows:

This paper proposes a plaque development degree recognition algorithm based on deep learning, which can judge and diagnose vascular diseases according to the degree of plaque development.

The rest of our paper was organized as follows. Related work was introduced in Section II. Section III described the CPCA algorithm proposed in this paper. Experimental results and analysis were discussed in detail in Section IV. Finally, Section V concluded the whole paper.

II. RELATED WORKS

A. MECHANISM OF ATHEROSCLEROSIS

The coronary artery is the most important blood supply system in the human heart. It consists of the left and right coronary arteries and their branches and is distributed on the epicedial surface to provide blood to the heart, as shown in Figure 1. Coronary artery disease (CAD) is also commonly known as coronary atherosclerotic heart disease. Due to severe atherosclerosis or spasm in the coronary arteries, coronary artery stenosis or obstruction, thrombosis, luminal occlusion, and ultimately unable to provide cardiac nutrition, resulting in myocardial blood supply, insufficient oxygen supply and myocardial infarction. Clinically, it is characterized by acute myocardial infarction, unstable angina pectoris, gangrene, thrombosis, and loss of peripheral function. It is a sudden, high-risk, high-cause cardiovascular disease.

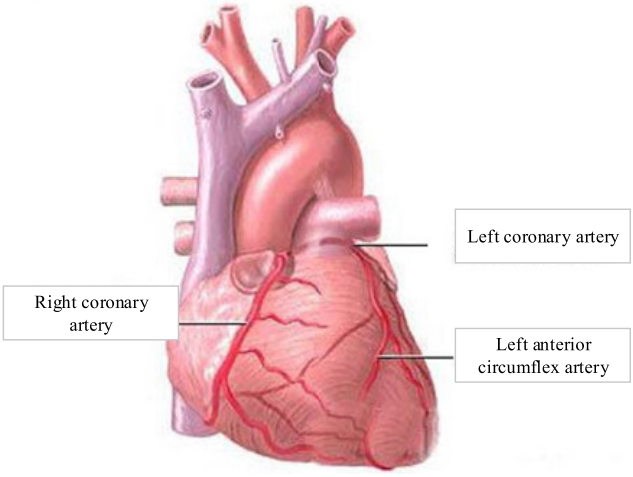

FIGURE 1. Schematic diagram of the coronary artery.

As one of the common predisposing factors for coronary heart disease, the specific pathogenesis of coronary atherosclerosis (AS) is complicated. It is recognized that the mature theory is the hypothesis of injury reflex [31], that is, blood includes a variety of chemical, mechanical, and biological factors, such as stimulation-induced endothelial cell injury, endothelial cell function and organic changes, and thereby damage the smoothness and integrity of the intima of arteries. At the same time, damaged cells can affect the normal metabolism of lipids in the body. In the blood, lipids usually enter the damaged area of the artery wall caused by endothelial cell damage, usually slowly settle down to the sub-intimal section, and deposit between smooth muscle cells and collagen and elastic fibers. Promote proliferation of smooth muscle cells. Smooth muscle cells and monocytes gradually engulf lipids in the blood and turn into foam cells. Lipoproteins are degraded into various substances such as cholesterol, cholesterol esters, and triglycerides. In addition, platelets can accumulate and adhere to damaged areas due to immune function. Exposed collagen activates platelets, which release a variety of growth promoting factors that allow endothelial and surrounding cells to proliferate in large Numbers. The formation of coronary atherosclerosis is a combination of various complex factors.

Coronary heart disease has been ranked among the top ten deadest diseases in the world and is one of the major harmful diseases of human health. The number of people suffering from coronary heart disease and dying from coronary heart disease is increasing and rejuvenating every year. In the past three decades of rapid economic development, the comprehensive construction of China's well-off society and the steady improvement of material living standards

have also accompanied the development of population aging. The number of patients with coronary heart disease in the middle-aged and elderly population is also increasing, and the prevention and treatment of coronary heart disease. It has become an important issue that cannot be ignored.

In recent years, scholars have divided the atherosclerotic plaque into stable and unstable plaques through extensive research [32], [33]. Moreover, a consensus has been reached on the pathological features of stable and unstable plaques. ''Unstable plaque'', also known as brittle plaque, has thin fibrous cap, large lipid necrosis center, more inflammatory cell infiltration, less extracellular matrix, smooth muscle cells and other pathological characteristics. This plaque is prone to rupture with thrombosis and causes an acute coronary event. Conversely, the ''stable plaque'' fiber cap thickness or lesion is mainly fibrous connective tissue, its lipid necrosis center is small or no matrix, smooth muscle cells are more, and inflammatory cells, macrophages are less, this plaque strength large, not easy to rupture, has a much smaller clinical impact. It can be seen that the stability of plaque is mainly related to its composition.

From a bioengineering point of view, the fibrous cap acts as a barrier between the lipid core and the blood and is an important factor affecting the stability of the plaque. Any factor that reduces the thickness of the fibrous cap or changes its matrix composition to reduce the mechanical strength of the blood flow can increase the instability of the plaque. In addition, the softer the plaque, the larger the lipid nucleus, the more stress it receives, and the more likely it is to rupture. Studies have shown that there are two main mechanisms for the formation of atherosclerotic plaque instability:

(1) The structure and morphology of the plaque itself change. In terms of structure, the fibrous cap becomes thinner and the core of lipid necrosis increases (>40%). In terms of morphology, the eccentric plaque is more unstable than the centripetal plaque, which is easier. When ruptured, its rupture is most likely to occur at the shoulder of the plaque, where the plaque moves with normal adjacent tissue.

(2) The mechanical stress acting on the plaque to trigger the rupture, that is, the physical, pathophysiological, and hemodynamic forces derived from the outside, which aggravates the instability of the plaque on the basis of the first aspect. For a particular plaque, relatively light changes such as avulsion, erosion, and fissures on the surface of the plaque may occur, and ulceration and rupture may occur. These lesions may be continuous or independent. Each can have serious clinical consequences.

In recent years, with the deepening of the study on the etiology and pathogenesis of coronary heart disease, the degree of plaque development plays an important role. The degree of plaque development is an important feature of atherosclerotic plaque. It can be seen that the degree of development in coronary atherosclerotic plaque plays an important role in coronary heart disease events. Therefore, in recent years, by detecting the degree of development of plaque, the instability of plaque can also be reflected.

B. DEEP CONVOLUTIONAL NEURAL NETWORK

In the 1990s, some scholars conducted research on convolutional neural networks and proposed a network model with acceptable performance. In recent years, with the improvement of computer hardware, the number of layers of convolutional neural networks has increased, and gradually developed into deep convolutional neural networks.

In order to enable the model to achieve better results in image classification, the training set is usually trained using a multi-layer backpropagation neural network. However, when using traditional BP neural network for image classification, we first manually perform complex feature extraction for each training sample, and then input the effective feature information in each training sample and perform iterative training repeatedly. Finally, the entire identification classification process is completed based on the weight and offset parameters that are finally trained.

If the image data after simple processing is directly used as the input information of the multi-layer BP neural network, it is bound to input unnecessary information together, resulting in a huge amount of information. As a result, under the extensive training conditions of the network model, the computational complexity of the network is exploding, and the computational efficiency is greatly reduced. If the number of training sets is reduced unilaterally, although the amount of calculation of the network will be reduced, it will easily lead to over-fitting, which makes the network have no good generalization performance.

The structure of the convolutional neural network is more complicated, mainly reflected in the convolutional neural network, which has two processes of convolution and down sampling. The neuron nodes of the convolutional neural network adopt a local perceptual field of view and weight sharing strategy, as well as the activation function and down sampling method to reduce the dimensionality of the data itself, so as not to reduce the main features of the information. Compared with multi-level BP neural network, it reduces the computational complexity of the network and improves the accuracy of recognition.

As shown in Figure 2, in the full connection, each neuron in the L1 layer and the neurons in the L0 layer are sequentially connected, and a total of 24 weight parameters are required. After using the local receptive field strategy, each neuron in the L1 layer is only connected to a part of the neurons in the L0 layer, so only 12 weight parameters are needed. Compared with the weighted parameter of the full connection, after using the local receptive field strategy, the number of weight parameters is reduced by half, which effectively reduces the amount of calculation.

Although the number of weight parameters required for the calculation can be effectively reduced after using the local receptive field strategy. However, as the identification needs advance, the number of layers of the convolutional neural network continues to deepen, and the number of parameters required for calculation is still very large. Therefore, the use of another weight sharing strategy is particularly important,

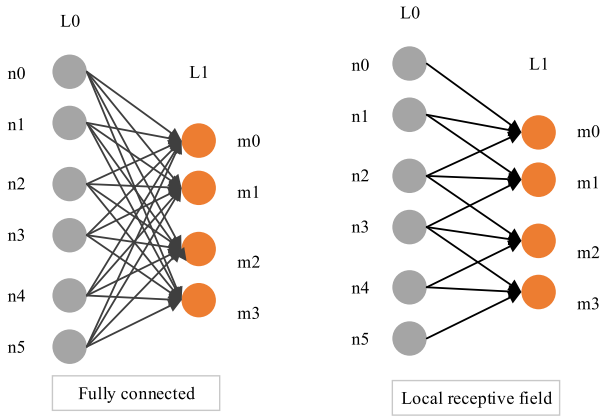

FIGURE 2. Schematic diagram of local perception field.

as shown in Figure 3. Before the weight sharing strategy is used in Figure 3, a total of 12 weight parameters are required to participate in the calculation from the L0 layer to the L1 layer. Each of the four neuron nodes in the L1 layer requires three different weights parameter. After the weight sharing strategy is adopted, only four weight parameters are required to participate in the calculation from the L0 layer to the L1 layer. Each of the four neuron nodes in the L1 layer needs only one weight parameter to share. Compared with the traditional full connection method, after using the local receptive field strategy and the weight sharing strategy, the weight parameter is reduced to one-sixth of the original, which greatly reduces the number of weight parameters and reduces the calculation amount.

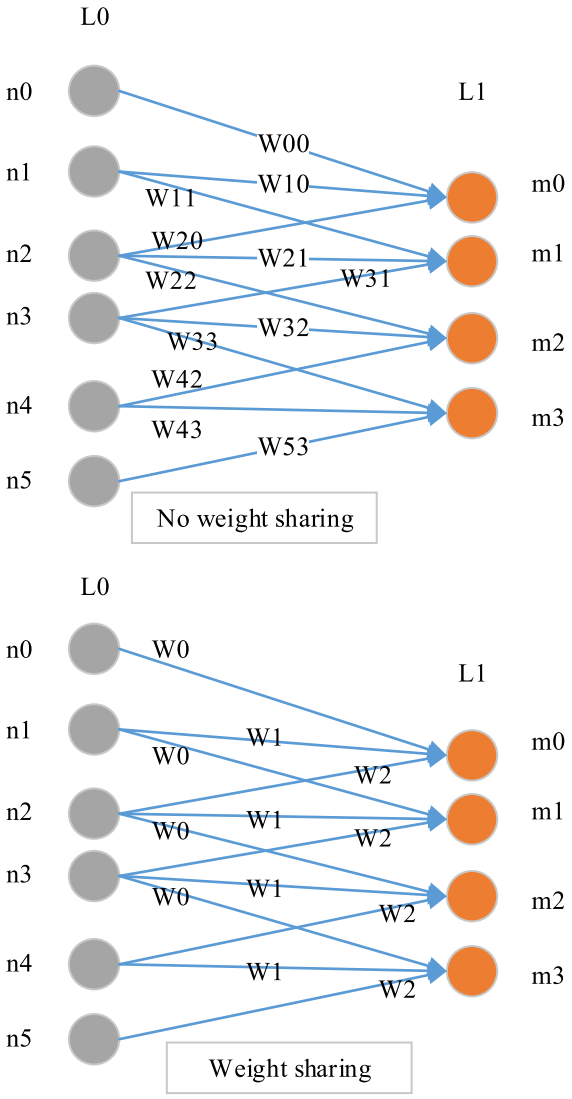

FIGURE 3. Schematic diagram of weight sharing.

The basic components of a convolutional neural network include the following five structures: convolutional layer, down sampling layer, fully connected layer, activation function, and loss function. The convolution layer performs a two-dimensional image convolution operation on the input image to achieve the purpose of extracting the feature image. The extracted image features are presented in the form of a feature map, and the number of feature maps is the same as the number of convolution kernels participating in the convolution calculation, that is, one convolution kernel corresponds to one feature map. The image convolution calculation process is shown in Figure 4.

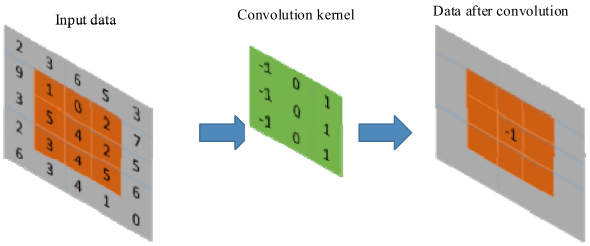

FIGURE 4. Image two-dimensional convolution calculation.

In Figure 4, the image size to be convolved is 5 × 5, and the convolution kernel size is 3 × 3. The convolution kernel slides on the image to be convolved, with a step size of one pixel per movement. When the convolution kernel slides to the position value on the image to be convolved in the figure, the nine parameters corresponding to the convolution kernel are respectively multiplied by the corresponding pixel feature points on the image to be convolved and finally summed, and the obtained calculation result is 3 × 3. The convolution feature value of the corresponding position in the feature map. Suppose the size of the image to be convolved is m × m, the size of the convolution kernel is k × k, and s stands for the step size of the convolution kernel sliding on the image, which is generated after convolution. The feature size is n × n, and there is a formula for calculating the feature size:

$$n = (m - k)/s + 1 \tag{1}$$

When m = 5, k = 3, s = 1, the calculation yields n = 3. In practical applications, in order to extract more features, more convolution kernels are usually used to extract features. This makes the input image not only have a large number

of feature images, but also the size of the feature image is relatively large after the feature image is extracted through the convolution layer. If the dimensionality reduction is not performed on the feature map, the subsequent calculation amount will increase, which will increase the computational complexity.

Therefore, it is necessary to continue to use the down sampling layer to perform dimension reduction processing on the extracted feature map, and reduce the image size of the feature map while reducing the main image information of the feature map. The purpose is to streamline the representative features of different regions in the map. The feature map is divided into multiple regions, and the maximum value in each region is calculated. This method is called maximum down sampling. As shown in Figure 5, after the image to be down sampled in the Figure 5 is divided into four regions, the size of each region is 2×2, and the maximum value in each region is calculated. If the feature map is divided into multiple regions, the way to solve the mean of each region is called mean down sampling. After down sampling, the feature map size is reduced to half of the original size.

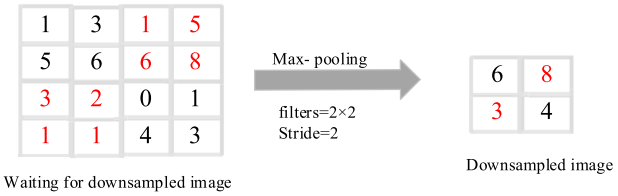

FIGURE 5. Maximum down sampling schematic.

After a series of convolutional layers are connected to the layers of the down sampling layer, they need to be connected to the fully connected layers to prepare for final identification and classification. The structure of the fully connected layer in the convolutional neural network is the same as that of the fully connected layer in the BP network structure. Each of the neuron nodes is connected to each other, and the input layer can be either a convolutional layer or a down sampling layer, and can be reasonably selected according to requirements.

Like traditional backpropagation neural networks, activation and loss functions are also essential in convolutional neural networks. The significance of using an activation function in a convolutional neural network is to preserve the characteristics of neurons that have been activated. That is, retain the required feature information and discard unnecessary information. Good nonlinear mapping capability is obtained. An activation function is typically used in the convolutional layer and the fully connected layer to preserve the characteristic information of the activated neurons [34]. The traditional activation functions mainly include the sigmoid function and the Tanh function. Its function image is shown in Figure 6.

$$f(x) = 1/(1 + e^{-x}) \tag{2}$$

$$f(x) = (e^{x} - e^{-x})/(e^{x} + e^{-x}) \tag{3}$$

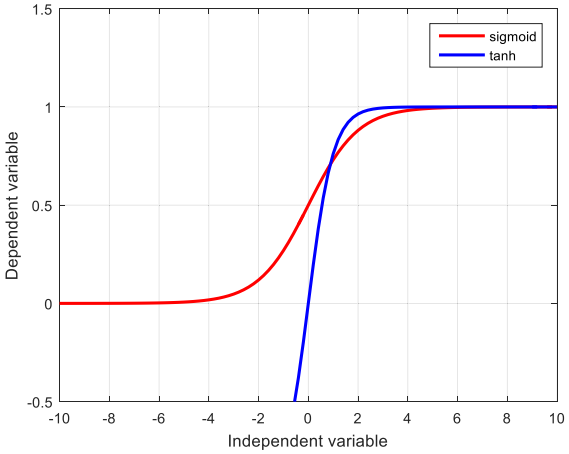

FIGURE 6. Sigmoid and Tanh activation function image.

The most widely used activation function in convolutional neural networks today is the Relu function. Its function image is shown in Figure 7.

$$f(x) = \max(0, x) \tag{4}$$

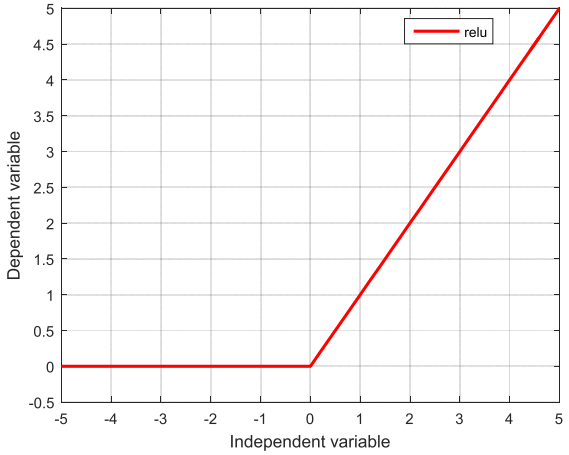

FIGURE 7. Relu activation function image.

After a series of calculations of the convolutional neural network, it is necessary to perform regression classification on the information of the output of the last layer as the fully connected layer of the network output, and the loss function is required in the process of regression classification. The commonly used loss functions in convolutional neural networks are: squared difference function and cross entropy function. The squared difference function is shown in equation (5):

$$C = (1/2)(\alpha - y)^2 \tag{5}$$

where C stands for the squared difference function, y is the expected output of the neuron and α is the actual output of the neuron. When the loss of neurons is proportional to the actual output and expected output gap, the cross entropy function formula is based on the entropy formula, and the calculated entropy is shown in equation (6).

$$H(y) = -\sum_{i} y_i \log(y_i) \tag{6}$$

where, the variable y is the expected output of the neuron. In the actual application, it is not known what statistical distribution the neuron expects output y will obey, so the distribution of y can only be estimated by calculating the actual output of the neuron. This way you can use α to represent the cross entropy of y as in equation (7):

$$H(y) = -\sum_{i} y_i \log(\alpha_i) \tag{7}$$

III. PATCH DEVELOPMENT RECOGNITION ALGORITHM BASED ON CPCA

A. SELECTION OF ROI AREA

The obtained two-dimensional carotid ultrasound image size is 576 × 768. Because the image size is large and contains a lot of useless information, 3 different types of ROI are selected according to the plaque development information, as shown in Figure 8.

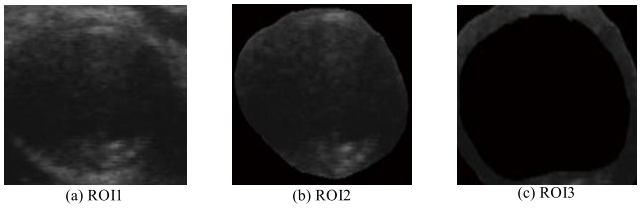

FIGURE 8. Three different types of ROI.

ROI1 is directly selected from the two-dimensional image according to the position of the blood vessel. When selected, the size of ROI1 is L × L.

$$L = \max\{x_{max} - x_{min}, y_{max} - y_{min}\} + 10 \tag{8}$$

where (x, y) is the coordinate information of the outer membrane.

ROI2 removes the tissue outside the adventitia based on ROI1, and the gray value outside the epicardium is set to zero.

ROI3 outlines the intima on the basis of ROI2, and the gray value in the inner membrane is set to zero.

B. SELECTION OF SLIDING NEIGHBORHOOD BLOCKS

As shown in Figure 9, based on the plaque region marked by the doctor, a sliding neighborhood block is established, such that its central pixel traverses each pixel of the plaque region, and extracts local features of the plaque region.

In order to analyze the influence of the size of the sliding neighborhood block on the patch recognition rate based on local features, the optimal size of the sliding neighborhood block is determined. In this study, multiple sizes are selected, which are 7 × 7, 9 × 9, 11 respectively. ×11, 13 × 13, 15 × 15, 17 × 17, and 19 × 19, and define the recognition accuracy (see equations (9) and (10)) to evaluate the effect of plaque recognition accuracy with different sizes of sliding neighborhood block pairs based on local features.

$$accuracy_i = N_{i_{pixCorr}} / N_{i_{totalROI}} \tag{9}$$

$$accuracy_{all} = \sum_{i=1}^{k} (N_{i_{pixTotal}} / N_{totalROI} \times accuracy_i) \tag{10}$$

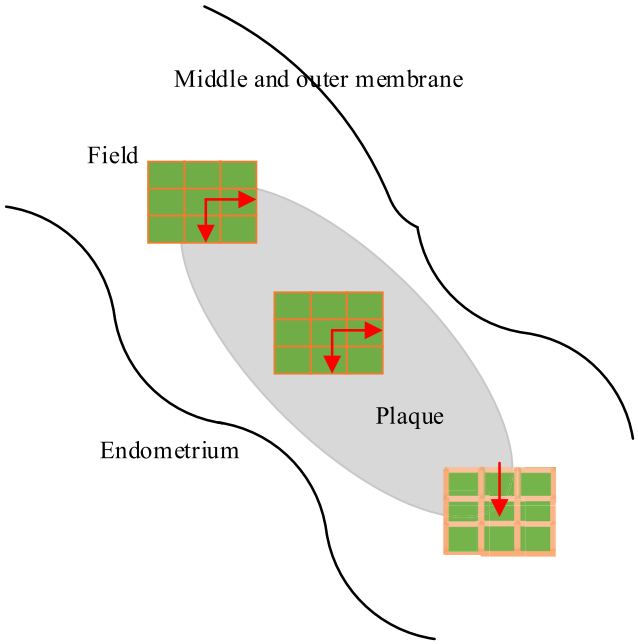

FIGURE 9. Schematic diagram of the 3 * 3 sliding neighborhood block traversing the entire plaque area.

Among them, the variable k represents the number of categories. The variable $accuracy_i$ is the recognition accuracy of i-th plaque sample block. The variable $N_{i_{pixCorr}}$ is the number of pixels of i-th plaque that is correctly classified. The variable $N_{i_{totalROI}}$ is the total number of pixels in i-th plaque sample block. The variable $accuracy_{all}$ is the overall recognition accuracy of the sample block. The variable $N_{i_{pixTotal}}$ is the total number of pixels of i-th plaque sample block. And the variable $N_{totalROI}$ is the total number of pixels of all sample blocks used for testing.

C. CPCA ALGORITHM

PCAnet [35] is a three-layer convolutional neural network that uses the principal component vector of training data as a feature of convolution kernel extraction. It is simpler than other convolutional network structures, without a pooling layer, with only two convolutional layers and one non-linear mapping layer. In addition, because the parameter learning in PCAnet does not require the use of backpropagation algorithms, and does not need to pre-train the convolution kernel through automatic encoder networks, deep confidence networks, etc., its training is very effective.

PCAnet was originally designed to give deep learning tasks, such as object recognition and image classification tasks in a variety of image datasets, a benchmark for experimental results through this simple model. However, experiments have shown that its images on multiple datasets. The classification results exceed the deep network of some complex designs, and also have good effects in texture classification and object recognition problems.

In PCAnet, the value of the pixel on the feature map is actually the expression coefficient of the dictionary based on the

PCA vector. Therefore, if we generate multiple sets of PCA vectors based on clustering, we can build an over complete dictionary and get the sparse expression of the small photo. Use this set of dictionaries can better express picture features. On the other hand, this idea is also inspired by the use of non-local features of the image for image slice clustering to complete the image restoration task [36]. We refer to the image slice clustering and the principal component analysis step by class as the pre-training of the cluster PCA network. The process is shown in Figure 10.

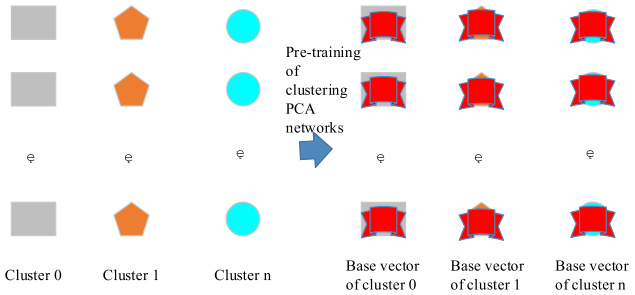

FIGURE 10. Pre-training steps for clustering PCA networks, divided into image slice clustering and principal component analysis by class.

Since we extracted small images at all positions of all the pictures, we can think that the small image set contains all the image information such as texture, corner, outline, etc. If the image can be classified according to this information, it can be executed by class. In order to better achieve image slice clustering, the image is firstly high-pass filtered, high-frequency images are extracted, and then small image slices are extracted in the high-frequency image domain, and then clustered. The reason for this is that high-frequency filters can enhance meaningful features in low-level image processing, and are used in image restoration problems to learn better dictionaries to express local features. In convolutional neural networks, convolution kernels have the same effect as dictionaries, so we combine this approach into clustered PCA networks.

Considering that the general ultrasound image data is a single-channel grayscale image, it is directly passed through a high-pass filter to operate on the grayscale domain, thereby extracting a small image slice. Moreover, features such as edges and textures of the image are highlighted by the high pass filter.

After acquiring the small image slice set, we use the following clustering rule: set the variance threshold, and divide all the small image slices whose variance is smaller than the threshold into the 0th class. These images are smooth pictures. Such an operation preserves meaningful feature images for subsequent clustering. Subsequently, we use k-means clustering for the remaining image slices, and set the number of clusters to N. Then the k-means algorithm aggregates the pieces with similar structure and features into N class. We use $Patch^i$ to represent i-th type of small picture set, combined with the 0th-type smooth set, all n + 1 clusters can be represented as a set:

$$\{Patch^0, Patch^1, Patch^2, \ldots, Patch^n\} \tag{11}$$

We perform principal component analysis on the small image slice sets in n + 1 clusters, respectively, and retain the first M principal component vectors as the dictionary of the class. For a small image slice of size $k_1 \times k_2$, using $PCA^i_{k1k2\times M}$ to represent the matrix of the first M principal component vectors of i-th cluster, we can represent the dictionary of n + 1 clusters as a large matrix:

$$\{PCA^0_{k1k2\times M}, PCA^1_{k1k2\times M}, PCA^2_{k1k2\times M}, \ldots, PCA^n_{k1k2\times M}\}_{k1k2\times(n+1)M} \tag{12}$$

Through this over-complete dictionary, clustering PCA networks can achieve sparse representation of images and adaptively select feature convolution kernels. So far, after getting the dictionary and cluster center, we completed the pre-training process of clustering PCA network.

When extracting picture features in forward propagation, we adopt the following strategy: for an input picture, first perform the fragmentation operation, and for each small image piece, find the corresponding class in n + 1 clusters. The specific method is to first determine whether the variance of the small image slice is less than the threshold. If it is determined to be a smooth picture, it is marked as cluster 0, otherwise it is calculated distance from the n cluster centers, and the nearest center is selected as the cluster. The small image slice has the same features and structure as the cluster image slice set, so the PCA vector group corresponding to the cluster can be used as the convolution kernel of the image slice. For a small image slice, if it belongs to cluster j, then you should select the dictionary from the over complete dictionary:

$$D = \{0^0_{k1k2\times M}, 0^1_{k1k2\times M}, 0^2_{k1k2\times M}, \ldots, 0^n_{k1k2\times M}\}_{k1k2\times nM} \tag{13}$$

Among them, the variable $0^i_{k1k2\times M}$ represents an all-zero matrix whose dimension is $k_1k_2 \times M$. Taking D as the convolution kernel, the corresponding expression coefficient of the small image piece can be obtained as follows:

$$[0, \ldots, p_{iM+1}, p_{iM+2}, \ldots, p_{iM+M}, \ldots, 0]_{nM} \tag{14}$$

We only take the expression coefficient corresponding to the PCA vector group corresponding to cluster j and put it into the corresponding position of the feature map. Clustering the second layer of the PCA network and the output layer are the same as PCAnet, and Figure 11 is a schematic diagram of its structure.

IV. EXPERIMENTS AND RESULTS

A. DATA SET AND IMAGE PREPROCESSING

The hardware of the experiment, using the DELL precision T5810 graphics workstation, equipped with Intel Xeon E5 2630 V3 processor and equipped with NVIDA Quadro

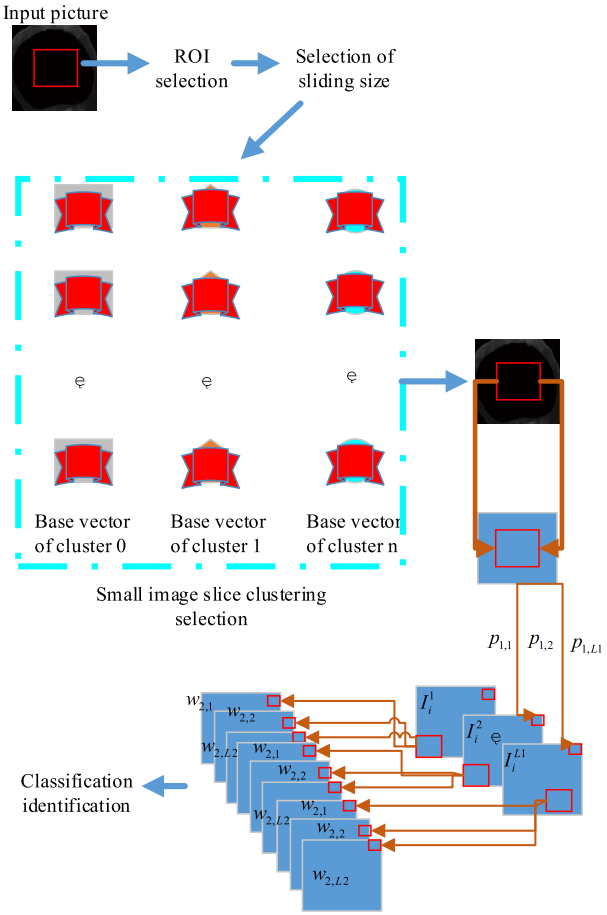

FIGURE 11. Schematic diagram of clustering PCA network.

K4200 graphics card, 4G memory, can support deep learning network training and testing. On the software side, windows 10 and ubuntu 16.04 dual systems are used, and programming software and languages are matlab 2013b and python. Use the tensorflow deep learning framework as the primary tool for building a network model.

The test image library used in this experiment was from the Seppoes Neuromedicine School. The image library did not contain serious lesions such as plaque. The image library contains 84 images from different testers. The testers ranged in age from 26 to 90 years with an average age of 52 years. Ultrasound images were acquired on an ATL HDI-3000 ultrasound scanner manufactured by Advanced Technology Laboratories, USA. The instrument is equipped with 64 high-resolution units and a 38 mm wide-band array. It uses multi-echo scanning technology. The scanning head operates at a frequency range of 4-7 MHz, a transmission focal length range of 0.8-1.1 cm, and an acoustic aperture of 10 × 8 mm. The acquired image has a resolution of 576 × 768 pixels, a pixel gray level of 256, and a pixel density of 16.66 pixels/mm.

In order to verify the reliability and generalization of the model, the data set is divided into training set and test set according to 4:1. At the same time, the images in the training set and test set must be from the IVUS image sequence of different patients. The test set does not participate in the training process. The purpose of this is to make the test set completely independent of the training set, so as to better evaluate the model results.

In the deep learning model, in order to avoid over-fitting, it is necessary to input sufficient data samples for learning, but usually the amount of medical image data and corresponding label data is often small, which cannot meet the requirements of a large number of data samples. Therefore, it is especially important to amplify the training data to improve the data capacity and increase the data characteristics to improve the generalization performance of the model. In terms of medical images, image geometric transformation is a common image amplification method. In this paper, we need to carry out image segmentation. In order to preserve the grayscale information and spatial information of the image as much as possible, we choose to rotate 90°, 180° and horizontal flip transform to amplify the data, which can make the data amount become 4 times of the original, corresponding to The label map also needs to be expanded accordingly. Data amplification was performed on the intima training data of the blood vessel and the original image and the label image of the three types of intravascular plaque training data, as shown in Figure 12.

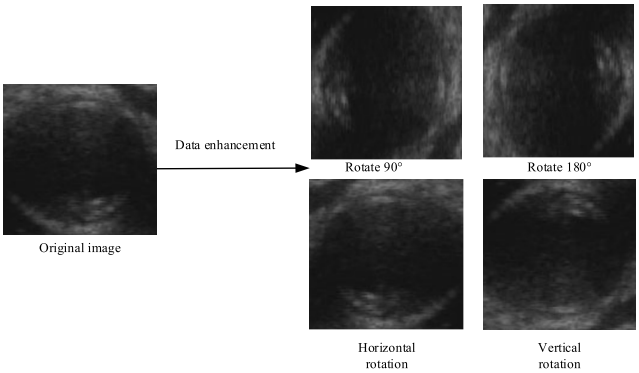

FIGURE 12. Data amplification.

B. INFLUENCE OF DIFFERENT ROI AREA SELECTION ON RECOGNITION PERFORMANCE

First, three different types of ROIs were trained and tested. The receiver operating characteristic (ROC) curve and the area under the curve (AUC) were used to evaluate the ability of the convolutional neural network trained with different types of ROI to identify the carotid plaque ultrasound images. The ROC curve is shown in Figure 13, and the area under the ROC curve is listed in Table 1.

As can be seen from Figure 13 and Table 1, ROI3 has the best recognition ability, and the AUC value is 0.981, which is much larger than ROI1 and ROI2. Therefore, accurate segmentation of the inner and outer membranes of the carotid artery has an important influence on the classification and recognition of the degree of plaque development. In addition,

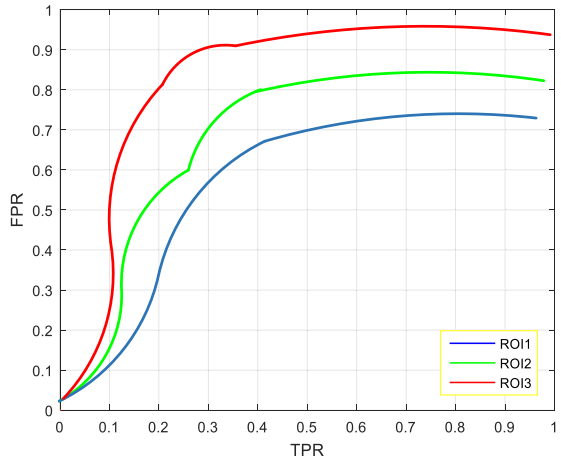

FIGURE 13. ROC curves for three types of ROI.

TABLE 1. Area values under three types of ROC curves.

The type of ROI	ROI1	ROI2	ROI3
AUC	0.812	0.871	0.981

it can be seen that the ROI2 of the outer membrane is slightly higher than the original ROI1. Due to the complexity of the ultrasound image itself, doctors usually determine the location of the blood vessel in the diagnosis of carotid atherosclerosis, and then use the degree of plaque development as an important indicator to determine atherosclerosis.

Finally, use ROI3 to train the network, take the parameters in the trained network as the initial value, use ROI1 as input to fine tune the network, and finally use the ROI1 test set to test. In this paper, the test result obtained by this method uses ROI3 + ROI1 to indicate. Similarly, the test results of ROI2 + ROI1, ROI3 + ROI2 + ROI1, ROI2 + ROI3 + ROI1 were obtained. The ROC curves obtained by different network training methods are shown in Figure 14, and the areas under the ROC curve are listed in Table 2. As can be seen from Figure 14 and Table 2, the ability to recognize the

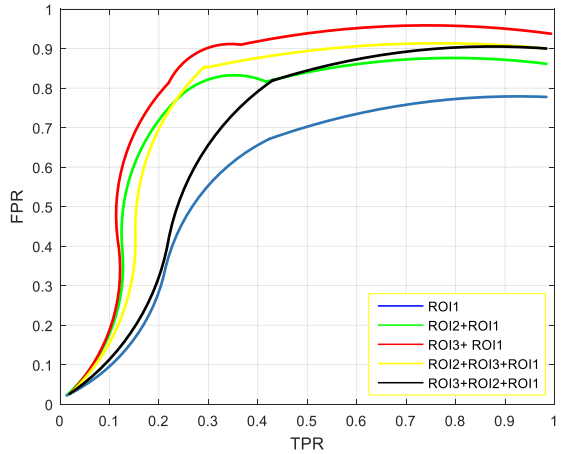

FIGURE 14. ROC curves for different network training methods.

TABLE 2. Area values under the ROC curve for different training methods.

Training method	AUC
ROI1	0.791
ROI2+ROI1	0.812
ROI3+ ROI1	0.886
ROI2+ROI3+ROI1	0.852
ROI3+ROI2+ROI1	0.846

degree of development of the carotid plaque ultrasound image can be improved. Among them, the ROI3 training network is used first, and the training result is obtained, then the network parameters are fine-tuned by ROI1, and the best recognition effect can be obtained, and the AUC value is 0.886. The AUC values obtained by ROI2 + ROI1, ROI3 + ROI2 + ROI1, ROI2 + ROI3 + ROI1 are not much different, but they are better than the original ROI.

C. INFLUENCE OF BLOCK SIZE IN SLIDING WINDOW AREA ON PLAQUE DEVELOPMENT DEGREE RECOGNITION PREPARATION RATE

In order to use the sample library more fully and reliably, the sample library is randomly divided into 5 parts, 4 parts are used as the training set of the classifier, and the remaining part is used as the test set of the classifier. A training group is formed by extracting 300 points from each of the four parts of the plaque sample; three different plaque samples are randomly selected from the remaining one part to form a test group, and five parts are rotated and trained. The overall recognition accuracy of each classifier for different sliding neighborhood blocks is calculated by equations (9) and (10).

In this study, the size of the sliding neighborhood block is: 7×7, 9×9, 11×11, 13×13, 15×15, 17×17, and 19×19. The results of the plaque development of the sliding neighborhood blocks of different sizes are shown in Figure 15 using the doctor's artificial marker results as the gold standard.

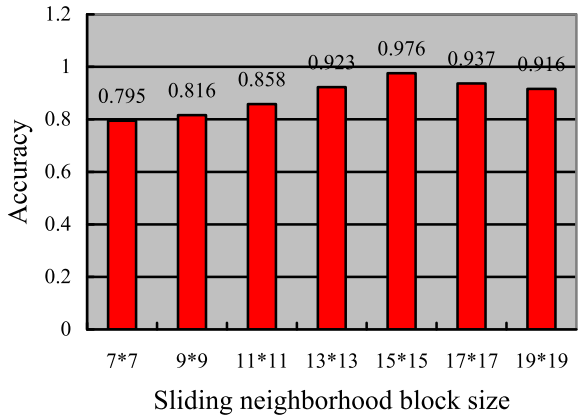

FIGURE 15. Relationship between sliding neighborhood blocks of different sizes and recognition accuracy.

As can be seen from Figure 15, as the size of the sliding neighborhood block increases, the plaque area gradually increases. Therefore, this paper selects a sliding neighborhood block with a pixel of 15 × 15 to perform local feature extraction on the plaque developing area of the test image.

D. COMPARISON OF CLASSIFICATION PERFORMANCE

In order to verify the recognition effect of the proposed algorithm on the plaque developed image, the identification of the plaque developed image database, the comparative literature [24], the literature [25], the literature [26], the PCAnet, the classical method SVM and the proposed algorithm CPCA are accurate rate. The recognition effect is shown in Table 3. The experiment was carried out under the same experimental conditions using the same equipment.

TABLE 3. Identification accuracy of different algorithms for plaque-developed images.

Methods	Training accuracy
Literature [24]	0.806
Literature [25]	0.902
Literature [26]	0.851
PCAnet	0.969
SVM	0.816
CPCA	0.976

It can be seen from Table 3 that compared with other algorithms, the proposed algorithm has better recognition effect on small sample plaque developed images, and the recognition performance is better than other algorithms. This is because this article first extracted different types of ROI for plaque images. Secondly, according to different ROI regions, the size of the sliding neighborhood block is determined, and a local feature image of the plaque developing region is further obtained. Then, by clustering PCA, multiple sets of convolution kernels are generated, and more plaque development features are extracted, so that the input image can adaptively select the feature extractor, and the recognition performance of the plaque development degree is improved.

In order to further verify the recognition ability of the proposed algorithm, the classification performance of these algorithms is compared by plotting the ROC curves of different algorithms. If the ROC curve is closer to the upper left corner, the closer the area under the curve is to 1, the better the classification effect of the algorithm, and vice versa. Figure 16 is a plot of ROC plotted against experimental results, and Table 4 is calculated for its corresponding AUC value.

As can be seen from Figure 16, the ROC curve of the CPCA algorithm proposed in this paper is mostly located at the upper left of other curves. The ROC curve for literature [24] and SVM is slightly higher than the diagonal, while the ROC curve for literature [25] is slightly higher than for literature [24] and SVM. It can also be seen from the AUC values calculated in Table 4 that the AUC value of CPCA

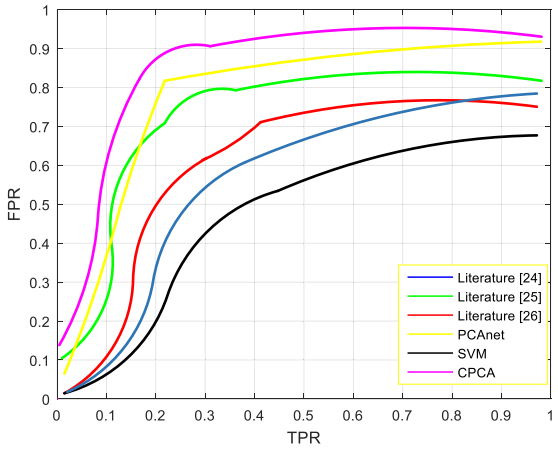

FIGURE 16. ROC graph with different algorithms.

TABLE 4. AUC values for different models.

Methods	AUC values
Literature [24]	0.815
Literature [25]	0.872
Literature [26]	0.832
PCAnet	0.912
SVM	0.751
CPCA	0.959

is 0.959 and the SVM is the lowest. Therefore, it can be seen that the ROC curve of the proposed algorithm is significantly better than the other algorithms.

In order to further verify the time performance of the proposed algorithm in this paper, this paper compared the use time of literature [24], literature [25], literature [26], PCAnet, classical method SVM and the proposed algorithm CPCA for test images. In the experiment, 10 test images were taken, and the average time of 10 test images was taken as the experimental result. The experimental results are shown in Table 5. It is obvious from table 5 that the time performance of the algorithm proposed in this paper is optimal.

TABLE 5. Times for different models.

Methods	Times(ms)
Literature [24]	623
Literature [25]	572
Literature [26]	532
PCAnet	712
SVM	831
CPCA	259

In conclusion, it can be found that the method proposed in this paper is superior to other models. This is because this paper first extracted different types of ROI for plaque images to improve the presence area of plaque targets. Secondly, according to different ROI regions, determine the size of

sliding neighborhood blocks, and then obtain a small picture of the patch development area, which can improve the operation efficiency of the network. Then, the small image is clustered, and the principal component vector is calculated according to the category, so as to generate multiple groups of convolution kernels and extract more features of patch development, so that the input image can select feature extractor adaptively, so as to realize classification and recognition with high efficiency and precision.

V. CONCLUSION

Convolutional neural networks have unique advantages in the field of speech recognition and image processing, and are also widely used in medical image processing. In this paper, angiographic contrast atherosclerotic plaques were used as the research object, and the convolutional neural network was applied to plaque development recognition. A plaque development degree recognition algorithm based on deep learning was proposed. First, different types of ROIs are extracted for plaque images. Secondly, according to different ROI regions, the size of the sliding neighborhood block is determined, and then a small image slice of the plaque developing area is obtained. Then, clustering small image slices, calculating principal component vectors by category, thereby generating multiple sets of convolution kernels, extracting more plaque developing features, so that the input images can adaptively select feature extractors, and then perform classification and recognition. The experimental results show that the proposed algorithm can judge and diagnose vascular diseases according to the degree of plaque development.

REFERENCES

[1] F. Burzotta, J. F. Lassen, T. Lefevre, D. Hildick-Smith, A. Chieffo, O. Darremont, M. Pan, Y. S. Chatzizisis, R. Albiero, Y. Louvard, and A. P. Banning, "Percutaneous coronary intervention in left main coronary artery disease: The 13th consensus document from the European Bifurcation Club," *Eurointervention*, vol. 14, no. 1, pp. 112–120, 2018.

[2] T. C. Lin, T. M. Lu, P.-F. Hsu, C.-C. Shih, S.-J. Lin, C.-P. Hsu, and F. C. Huang, "Coronary artery bypass surgery versus percutaneous coronary intervention for left main coronary artery disease with chronic kidney disease," *Int. Heart J.*, vol. 59, no. 2, pp. 279–285, 2018.

[3] K. Vaidya, C. Arnott, G. J. Martínez, B. Ng, S. McCormack, D. R. Sullivan, D. S. Celermajer, S. Patel, "Colchicine therapy and plaque stabilization in patients with acute coronary syndrome: A CT coronary angiography study," *JACC, Cardiovascular Imag.*, vol. 11, no. 2, pp. 305–316, 2018.

[4] M. Faraji, I. Cheng, I. Naudin, and A. Basu, "Segmentation of arterial walls in intravascular ultrasound cross-sectional images using extremal region selection," *Ultrasonics*, vol. 84, pp. 356–365, Mar. 2018.

[5] S. S. Kim, M. H. Yamamoto, N. Sidik, K. Koyama, C. Berry, K. G. Oldroyd, G. S. Mintz, M. McEntegart, and A. Maehara, "Intravascular ultrasound assessment of the effects of rotational atherectomy in calcified coronary artery lesions," *Int. J. Cardiovascular Imag.*, vol. 34, no. 9, pp. 1365–1371, 2018.

[6] R. W. Jones, G. R. Parkerson, P. A. Armstrong, N. Moudgill, M. R. Back, P. Inkyong, J. Brooks, and D. T. Fontenot, "IP111. A role for intravascular ultrasound as an adjunct to therapeutic decision-making during carotid artery stenting," *J. Vascular Surg.*, vol. 67, no. 6, pp. e117–e118, 2018.

[7] Z. Li, L. Wang, P. Zhang, Y. Chen, X. Liu, M. Xu, H. Su, M. Zhang, and X. Hu, "Intravascular ultrasound elastography analysis of the elastic mechanical properties of atherosclerotic plaque," *Int. J. Cardiovascular Imag.*, vol. 33, no. 5, pp. 1663–1671, 2017.

[8] F. Chen, R. Ma, J. Liu, M. Zhu, and H. Liao, "Lumen and media-adventitia border detection in IVUS images using texture enhanced deformable model," *Comput. Med. Imag. Graph*, vol. 66, pp. 1–13, Jun. 2018.

[9] C. V. Bourantas, T. Zanchin, A. Karagiannis, A. Ramasamy, K. Yamaji, M. Taniwaki, D. Heg, A. Moschovitis, D. Fotiadis, L. Mihalis, and A. Sakellarios, "Implications of the local haemodynamic forces on the phenotype of coronary plaques," *Heart*, vol. 105, no. 14, pp. 1078–1086, 2019.

[10] A. Taneja, P. Ranjan, and A. Ujlayan, "An efficient SOM and EM-based intravascular ultrasound blood vessel image segmentation approach," *Int. J. Syst. Assurance Eng. Manage.*, vol. 7, no. 4, pp. 442–449, 2016.

[11] Y. Gao, Z. Liang, H. Zhang, M. J. Pomeroy, J. A. Ferretti, T. V. Bilfinger, J. Ma, H. Lu, and W. H. Moore, "A feasibility study of extracting tissue textures from a previous full-dose CT database as prior knowledge for Bayesian reconstruction of current low-dose CT images," *IEEE Trans. Med. Imag.*, vol. 38, no. 8, pp. 1981–1992, Aug. 2019.

[12] M. J. Lian and C. L. Huang, "Texture feature extraction of gray-level co-occurrence matrix for metastatic cancer cells using scanned laser pico-projection images," *Lasers Med. Sci.*, vol. 34, no. 7, pp. 1503–1508, 2019.

[13] H. Liu, G.-F. Xiao, C.-J. Ouyang, and Y. L. Tan, "Multi-source remote sensing image registration based on contourlet transform and multiple feature fusion," *Int. J. Autom. Comput.*, vol. 16, no. 5, pp. 575–588, 2019.

[14] A. Rocha and S. K. Goldenstein, "Multiclass from binary: Expanding one-versus-all, one-versus-one and ecoc-based approaches," *IEEE Trans. Neural Netw. Learn. Syst.*, vol. 25, no. 2, pp. 289–302, Feb. 2014.

[15] F. Sampedro, S. Escalera, and A. Puig, "Iterative multi-class multi-scale stacked sequential learning: Definition and application to medical volume segmentation," *Pattern Recognit. Lett.*, vol. 46, no. 46, pp. 1–10, 2014.

[16] D. Kwon, H. Kim, S. C. Suh, I. Kim, K. J. Kim, and J. Kim, "A survey of deep learning-based network anomaly detection," *Cluster Comput.*, vol. 22, no. 5, pp. 949–961, 2019.

[17] Q. Dong, S. Gong, and X. Zhu, "Imbalanced deep learning by minority class incremental rectification," *IEEE Trans. Pattern Anal. Mach. Intell.*, vol. 41, no. 6, pp. 1367–1381, Jun. 2019.

[18] S. Peng, H. Jiang, and H. Wang, "Modulation classification based on signal constellation diagrams and deep learning," *IEEE Trans. Neural Netw. Learn. Syst.*, vol. 30, no. 3, pp. 718–727, Mar. 2019.

[19] Q. Xia, S. Li, A. M. Hao, and Q. P. Zhao, "Deep learning for digital geometry processing and analysis: A review," *J. Comput. Res. Develop.*, vol. 56, no. 1, pp. 155–182, 2019.

[20] J. Yao, J. Wang, Y. Zhang, J. Sun, C. Zhang, R. Zhang, and I. W. Tsang, "Deep learning from noisy image labels with quality embedding," *IEEE Trans. Image Process.*, vol. 28, no. 4, pp. 1909–1922, Apr. 2019.

[21] T. Matsubara, T. Ochiai, T. Akutsu, J. C. Nacher, and M. Hayashida, "Convolutional neural network approach to lung cancer classification integrating protein interaction network and gene expression profiles," *J. Bioinf. Comput. Biol.*, vol. 17, no. 3, pp. 3066–3072, 2019.

[22] G. Litjens, T. Kooi, B. E. Bejnordi, A. A. A. Setio, F. Ciompi, M. Ghafoorian, Jeroen A. W. M. van der Laak, B. van Ginneken, and C. I. Sánchez, "A survey on deep learning in medical image analysis," *Med. Image Anal.*, vol. 42, no. 9, pp. 60–88, 2017.

[23] Z. Li, Z. Hou, Z. Hao, Y. An, S. Liang, B. Lu, and C. Chen, "Automatic cardiothoracic ratio calculation with deep learning," *IEEE Access*, vol. 7, pp. 37749–37756, 2019.

[24] T. Araki, N. Ikeda, N. D. Londhe, V. K. Shrivastava, S. K. Banchhor, L. Saba, A. Nicolaides, S. Shafique, J. R. Laird, J. S. Suri, and D. Shukla, "A new method for IVUS-based coronary artery disease risk stratification: A link between coronary & carotid ultrasound plaque burdens," *Comput. Methods Programs Biomed.*, vol. 124, pp. 161–179, Feb. 2016.

[25] G. Shi, Y. He, B. Yin, L. Zuo, P. She, W. Zeng, and F. Ali, "Analysis of mutual couple effect of UHF RFID antenna for the Internet of Things environment," *IEEE Access*, vol. 7, pp. 81451–81465, 2019.

[26] F. Hoseini, A. Shahbahrami, and P. Bayat, "AdaptAhead optimization algorithm for learning deep CNN applied to MRI segmentation," *J. Digit. Imag.*, vol. 32, no. 1, pp. 105–115, 2019.

[27] J. Hamwood, D. Alonso-Caneiro, S. A. Read, S. J. Vincent, and M. J. Collins, "Effect of patch size and network architecture on a convolutional neural network approach for automatic segmentation of OCT retinal layers," *Biomed. Opt. Express*, vol. 9, no. 7, pp. 3049–3066, 2018.

[28] S. Soffer, A. Ben-Cohen, M. M. Amitai, H. Greenspan, E. Klang, and O. Shimon, "Convolutional neural networks for radiologic images: A radiologist's guide," *Radiology*, vol. 290, no. 3, pp. 590–606, 2019.

[29] S. Bao and A. C. S. Chung, "Multi-scale structured CNN with label consistency for brain MR image segmentation," *Comput. Methods Biomech. Biomed. Eng., Imag. Vis.*, vol. 6, no. 1, pp. 113–117, Jan. 2018.

[30] S. Lu, F. Jian, H. Zhang, J. Liu, and Z. Wu, "An estimation method of defect size from MFL image using visual transformation convolutional neural network," *IEEE Trans. Ind. Informat.*, vol. 15, no. 1, pp. 213–224, Jan. 2019.
[31] J. Liu, Y.-H. Wang, L. Liu, H. Yang, P. Meng, and Y.-S. Han, and W. Li, "Structural and functional damage to the hippocampal neurovascular unit in diabetes-related depression," *Neural Regener. Res.*, vol. 14, no. 2, pp. 289–297, 2019.
[32] D. Shishikura, Y. Kataoka, K. Takata, S. W. Kim, J. Andrews, P. J. Psaltis, M. Sweeney, E. Kulikowski, J. Johansson, N. C. W. Wong, S. J. Nicholls, and S. Honda, "The effect of bromodomain and extra-terminal inhibitor apabetalone on attenuated coronary atherosclerotic plaque: Insights from the ASSURE trial," *Amer. J. Cardiovascular Drugs*, vol. 19, no. 1, pp. 49–57, 2019.
[33] S. Okuchi, Y. Fushimi, A. Yamamoto, T. Okada, T. Kikuchi, K. Yoshida, S. Miyamoto, K. Togashi, and T. Okada, "Visualization of carotid vessel wall and atherosclerotic plaque: T1-SPACE vs. compressed sensing T1-SPACE," *Eur. Radiol.*, vol. 29, no. 8, pp. 4114–4122, 2019.
[34] L. Chen, H. Qu, J. Zhao, B. Chen, and J. C. Principe, "Efficient and robust deep learning with correntropy-induced loss function," *Neural Comput. Appl.*, vol. 27, no. 4, pp. 1019–1031, May 2016.
[35] F. C. Soon, H. Y. Khaw, J. Kanesan, and J. H. Chuah, "PCANet-based convolutional neural network architecture for a vehicle model recognition system," *IEEE Trans. Intell. Transp. Syst.*, vol. 20, no. 2, pp. 749–759, Feb. 2019.
[36] S. Li and H. Qi, "A Douglas–Rachford splitting approach to compressed sensing image recovery using low-rank regularization," *IEEE Trans. Image Process.*, vol. 24, no. 11, pp. 4240–4249, Nov. 2015.

JINYONG ZHAN graduated from the Bengbu Medical College, in 2013. He is currently working with HwaMei Hospital, University of Chinese Academy of Sciences. His research interest includes vascular ultrasound diagnosis, especially the diagnosis of carotid atherosclerosis.

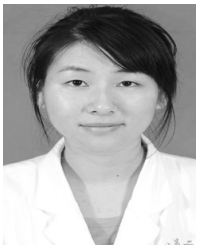

JUE WANG graduated from the Zhejiang University School of Medicine, in 2019. She is currently working with HwaMei Hospital, University of Chinese Academy of Sciences. Her research interest includes vascular ultrasound diagnosis, especially the diagnosis of carotid atherosclerosis.

ZHIFEI BEN graduated from Wenzhou Medical University, in 2017. In 2018, he served as the Deputy Director of the Youth Committee of the Ultrasound Medical Branch, Zhejiang Medical Association. He is currently working with HwaMei Hospital, University of Chinese Academy of Sciences. His research interest includes vascular ultrasound diagnosis, especially in the field of atherosclerosis.

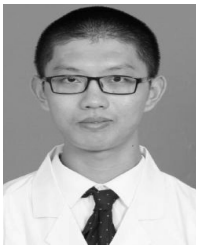

HAIDONG RUAN graduated from the Shantou University Medical College. He is currently working with HwaMei Hospital, University of Chinese Academy of Sciences. His research interest includes cardiovascular ultrasound, especially atherosclerosis.

SAIJUN CHEN graduated from Wenzhou Medical University, in July 2001. In 2018, she served as the President of the Ningbo Ultrasonic Medical Engineering Society. She is currently working with HwaMei Hospital, University of Chinese Academy of Sciences. Her research interest includes cardiovascular ultrasound, especially in atherosclerosis.